Available online at www.sciencedirect.com

ScienceDirect

journal homepage: www.elsevier.com/locate/he

A metal hydride compressor for a small scale H_2 refuelling station

Jussara Barale [a,1], *Federico Nastro* [b,2], *Davide Violi* [a], *Paola Rizzi* [a,*], *Carlo Luetto* [b], *Marcello Baricco* [a]

[a] *Department of Chemistry and NIS - INSTM, University of Turin, Via Pietro Giuria 7, 10125, Torino, Italy*
[b] *Tecnodelta S.r.l., Via Francesco Parigi 5H, Chivasso (To), 10034, Italy*

HIGHLIGHTS

- A prototype of metal hydride compressor was released based on commercial alloys.
- The MHC compressed hydrogen from 28 bar to 250 bar between RT and 150 °C.
- The MHC is integrated with an electrolyser driven by photovoltaic panels.
- The optimized compression process results in an average H_2 flowrate of 104 Nl/min.

GRAPHICAL ABSTRACT

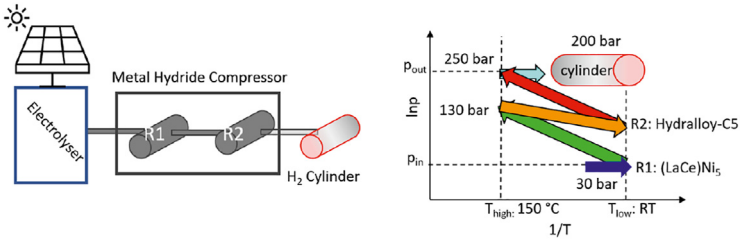

ARTICLE INFO

Article history:
Received 4 April 2023
Received in revised form
8 May 2023
Accepted 14 May 2023
Available online 31 May 2023

Keywords:
Metal hydride compressor
Intermetallic compounds
Metal hydride
Hydrogen refuelling station

ABSTRACT

The use of hydrogen as energy vector implies the development of the necessary infrastructures for hydrogen handling. A two-stage metal hydride compressor was developed and integrated in a small-scale hydrogen refuelling station at prototype level. In this work, the compression on site of green hydrogen using metal hydrides is exhaustively presented taking into account all the necessary aspects to bridge the gap between the laboratory and the real application. In particular, all aspects for the setting up of a metal hydride compressor, *i.e.* selection and characterization of selected metal hydrides, sizing of the plant components, design and the tests aimed to optimize the working performances are presented and deeply discussed, including energy consumption and efficiency necessary to build up a commercial system. The compressor employs two commercial alloys, *i.e.* a $La_{0.9}Ce_{0.1}Ni_5$ from Labtech in the first stage and the Hydralloy-C5 from GfE in the second one. Working between room temperature for absorption and 150 °C for desorption, the hydrogen produced by the electrolyser at 28 bar is compressed up to 250 bar, resulting in a compression ratio of about 9. The metal hydride compressor has a final power consumption of 614 W, of which 85 W are linked to the hydrogen sorption reactions, while other contributions come from the pumps involved in the plant and the dissipations. The

* *Corresponding author*. 9, Via P. Giuria 9, 10125, Torino, Italy.
E-mail address: paola.rizzi@unito.it (P. Rizzi).
[1] Present address: Tecnodelta S.r.l., Via Francesco Parigi 5H, 10,034 Chivasso (To), Italy.
[2] Present address: Nippon Gases Italia S.r.l, Via Marie Curie, 134/A, 10,034 Chivasso (To), Italy.

https://doi.org/10.1016/j.ijhydene.2023.05.155

compressor presents an isentropic efficiency of about 11% for less than 1 kg of powder in each stage and an average H_2 flowrate of 104 Nl/min is observed. The performances of the plant were optimized and maintained for a working time of about 245 h.

Introduction

In spreading the use of hydrogen as an energy vector, its compression still plays a key role, since the gas phase is the most widely used method to handle hydrogen [1]. The existing storage cylinder allow to store H_2 up to 200 bar (type I), but, since high pressures are required to store a large amount of H_2 in a small volume, tanks with pressures up to 700 bar are also available (type III and IV) [2]. As an example, hydrogen refuelling stations (H2RS) for cars need to deliver H_2 over 700 bar, *i.e.* the pressure required on board, while 350 bar are necessary for buses [3]. Indeed, the higher is the pressure on board, the higher is the amount of stored H_2 and the longer are the distance that can be covered [3]. Nowadays, conventional mechanical compressors are widely used, since they allow to face the high pressure required by applications. Nevertheless, these technologies imply loss in heat, high energy consumption and high maintenance costs, resulting one of the main investment for a refuelling station [1,4,5]. To overcome these problems, several non-mechanical technologies are considered as alternatives, *i.e.* electrochemical, cryogenic, adsorption and thermally powered compressors based on metal hydride (MH) [1,6,7].

For the latter technology, compression occurs thanks to the thermodynamic of the equilibrium of the reversible reaction between a metal/alloy and H_2 to form MH and heat. The equilibrium implies that at low temperatures correspond low pressures, while at high temperatures, pressures increase. Thus, the compression occurs since H_2 is absorbed at low temperatures (T_{low}) and low pressures, forming a MH, and afterwards, by heating the MH at higher temperatures (T_{high}), H_2 is released at a pressure considerably higher than absorption. Afterword, H_2 can be stored or further compressed by another stage. Thanks to their thermodynamic properties, MH obtained from intermetallic compounds (*e.g.* TiFe-based, $TiMn_2$-based and $LaNi_5$-based) are usually considered, [1,8]. Metal hydride compressors have several advantages, *e.g.* no moving parts, low maintenance, implying low Operational Expenditure costs (OPEX), and easy design [8,9]. Moreover, a high purity compressed gas is delivered. This technique is even promising from an environmental point of view, when waste heat can be used instead of electricity [10].

In the past years, the feasibility of MHs to compress H_2 was widely proven through a series of laboratory scale compressors, reaching delivery pressure above 350 bar [11–22]. Nevertheless, few examples exist at the prototype level and even fewer are commercially available. The commercial items and prototype systems proposed till now can work generally between room temperature in absorption up to a maximum of 150 °C, delivering a pressure up to 200–250 bar [9,23,24]. A commercially available compressor is the compact HyCo developed by GRZ Technologies for laboratory purposes [9,23]. The Norwegian company HYSTORSYS AS [24] provides compressors able to release up to 250 bar at 150 °C, with an hydrogen flow up to 30 Nm^3/h, depending on client needs [25]. A common use of MH compressors is the integration in H2RS, and a representative example is the systems built for the refuelling of forklifts in South Africa at the HySA laboratory [26] and in Croatia, in the framework of the project HYDRIDE4MOBILITY, in which MH compressors were provided by HYSTORSYS AS [24,27]. The latter company provided a first compression stage of a refuelling station for cars in Lillestrøm (NO), in substitution of a diaphragm compressor [25,28]. The HYSTORE Technology Ltd developed a prototype of a compressor that delivers H_2 at 220 bar by working at moderate temperature, *i.e.* 80 °C, allowing the use of water as thermal fluid [17]. In Ref. [29], a high-pressure MH compressor was presented, with an output pressure of 414 bar at about 130 °C.

Commercial/prototype systems reported above have in common the use of IMCs with not declared compositions, which are often not available on the market, but a private and specific production is inferred for these systems [17,23–25,27,29]. This is not advantaging for an industrial scale production of MH compressors, since it implies the need of a large quantity of powders, that can be obtained only by an industrial production. The advantage of realizing prototypes based on already commercially used compounds is their availability, allowing an easy scaling up and introduction on the market. To our knowledge, only one example is present in the literature in which the use of commercial hydrides powder was explicitly mentioned: the MH compressor realized thanks to $LaNi_5$ and $La_{0.5}Ce_{0.5}Ni_5$ IMCs acquired from the Whole Win company [30]. By using these commercial alloys, H_2 is released at 150 bar and 150 °C and the compressor has a size for medium/large scale applications [30].

In this work, a green hydrogen refuelling station was designed and tested to exploit the production and compression onsite of H_2 at 200 bar in a 3.0 l tank, corresponding to 600 l in normal conditions and about 54 g of hydrogen. This amount of hydrogen was produced being in line with quantities suitable for light mobile applications, like drones. Considering a PEM fuel cell consuming 0.8 Nm^3 of hydrogen per kWh produced, this corresponds to an energy content of about 0.75 kWh, allowing a drive time of 1 h for a drone with a power of 750 W. In fact, the market of drones is now attracted by the hydrogen technologies thanks to the higher energy density compared to batteries [31], allowing to reach higher time of flights. The higher is the pressure and the amount of hydrogen stored, the higher is the time of flight and the smaller is the required volume. As an example, Intelligent Energy for a 650 W Fuel Cell expects a time of flights of 85 min

with 2.0 l of compressed H_2 (pressure not given) with 256 W h/kg [32].

This work aims to show the feasibility of a completely green H2RS based on renewable energies, exploiting the production of H_2 by an electrolyser (EL) driven by photovoltaics (PV) and a MH compressor based on commercial alloys, working between room temperature and a maximum of 150 °C [17,23–25,27,29]. The work includes a market survey to find suitable commercial materials that can fit the requirement of pressure (*i.e* ≥ 200 bar, between room temperature and 150 °C). On the basis of selected alloys, their characterization, the MH compressor design and building, and its integration in the H2RS have been performed. Tests aimed to optimize the process according to plant design will be presented. Finally, the alloys were analysed after their use in the plant to detect possible chemical and properties variations.

Experimental

The selected IMCs are the $La_{0.9}Ce_{0.1}Ni_5$ commercialized by LabTech and the Hydralloy-C5 produced by Gfe. Alloys were studied before and after their usage in the MH compressor. The structural and morphological characterization of the commercial alloys was performed by Scanning Electron Microscopy (SEM) and Powder X-Ray Diffraction (PXD) analysis. Alloys were characterized as loose powder with a SEM instrument Tescan Vega, by acquiring secondary electron (SE) images for the morphological study, while Energy Dispersive X-ray (EDX) elemental maps were acquired at 20 keV. Powders were analysed with a X'Pert Pro diffractometer in Debye-Scherrer geometry, equipped with Cu-Kα source and X'celerator detector. The powder samples were manually grinded in a mortar and packed in glass capillaries with a diameter of 0.8 mm. Measurements were performed with steps of 0.016°, from 25° to 135° in 2θ, time per scan of 130 s, for the $(LaCe)Ni_5$; and from 25° to 100° in 2θ, time per scan of 250 s, for the Hydralloy-C5. Qualitative analyses of the PXD patterns were performed with the software X-Pert High Score, while the Rietveld refinements of the crystal structures were carried out with the software Maud [33]. Finally, the hydrogen sorption measurements were performed with pressure-composition-temperature (pcT) curves in a Sievert's type apparatus from the AMC of Pittsburgh, where temperature is controlled through an electric furnace. Pure hydrogen 6.0 commercialized by Nippon gases was used.

Results and discussion

H_2 refuelling station design

The developed small-scale refuelling station provides H_2 at a pressure ≥200 bar, exploiting electrolysis driven by PV and compression based on MH, charging a 3.0 l type IV cylinders. The H2RS consists of three main parts, as schematically shown in Fig. 1.

1) The EL hydrogen production, integrated with the PV panels.
2) The compression stage composed of the MH compressor.
3) The high-pressure storage, *i.e.* the 3.0 l cylinder.

Concerning the production of H_2, after a market survey, evaluating EL performances in terms of delivery pressure, working temperature, the feasibility to be integrated with PV panels (PVP), output H_2 flow and costs, the EL model *EL250* commercialized by Enapter was selected. It is an alkaline EL, based on KOH, which produces H_2 at 35 bar, working from 5 °C to 45 °C, and presenting an output H_2 flow of about 250 Nl/h and an operative power consumption of 1.3 kW. It can be supplied by grid current or by PVPs. At 35 bar, the producer declared an output H_2 purity of 99.94% with oxygen and water expected as contaminants. In particular, the producer advices about 600 ppm of water in the outer H_2 gas at 30 bar, while, at the same outlet pressure, there are no data available concerning the oxygen content. To increase the purity of the outer gas, a homemade purification stage was integrated at the outlet of the EL, that consists of a stainless-steel tube filled with *Zeolite 13X*, to reduce the amount of water, thanks to its adsorption. The EL was supplied with a PV plant that, in order

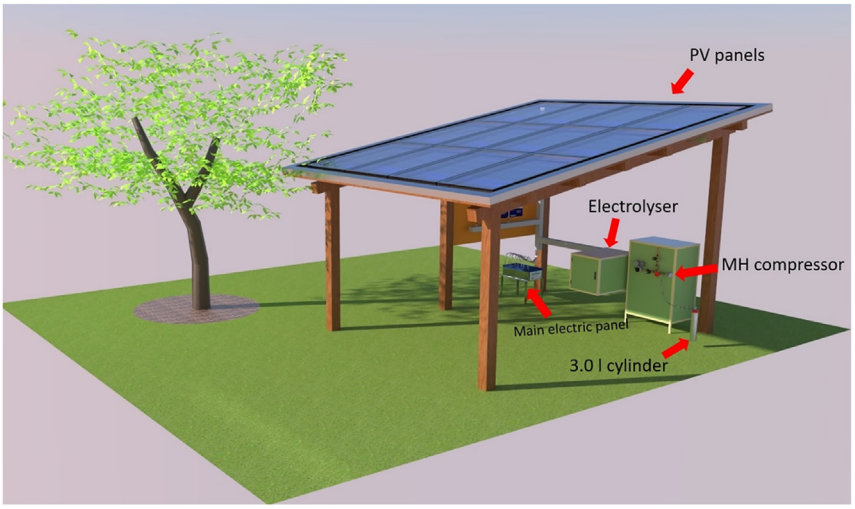

Fig. 1 – Schematic representation of the hydrogen refuelling station.

to provide the necessary amount of power, was sized with 10 panels of 300 W, commercialized by Hanover Solar.

The compressor was designed on the basis of the EL characteristics and on the assumption that the flow of H_2 must be spontaneous, due to the exploitation of a different pressure among various stages. This implied that the MH needs to absorb H_2 directly form the EL at pressure $\leq$30 bar. Furthermore, it was important to fix the values of temperature in absorption (T_{low}) and desorption (T_{high}). For T_{low}, Room Temperature (RT), *e.g.* about 20–30 °C, was selected, to have a similar working temperature of the EL, avoiding any cooling or heating step. For T_{high}, 150 °C was chosen, in line with commercially available or prototypes of MH compressors realized so far [23–25,27,30,34].

Alloys' selection and characterization

Market survey and selection of alloys

The selection of proper alloys involved a market survey of commercially available IMCs among producers at international level (*e.g.* Whole Win, GKN, JMC, LabTech, Gfe). The equilibrium pressures at the T_{low} and T_{high} were estimated by applying the Van't Hoff equation [8], using values of $\Delta H_{abs/des}$ and $\Delta S_{abs/des}$ reported in the literature and/or declared by producers for the considered compositions. From the market survey, it was evident that about 250 bar can be achieved at 150 °C with the Hydralloy-C5, commercialized by Gfe. It is an $TiMn_2$ IMC, that has, as a drawback, to be sensitive to O_2 and H_2O contaminations [8]. Since the H_2 produced by the EL contains both O_2 and H_2O, as previously described, it was necessary to design a first absorption stage using an alloy more resistant to the impurities present in the gas supply working as a purification, since during the desorption stage only hydrogen is released, while contaminants are reacting with the material. The $La_{0.9}Ce_{0.1}Ni_5$ alloy commercialized by LabTech was selected, which is a $LaNi_5$-based alloy [8] with high resistance to impurities and a low equilibrium pressure at T_{low} in absorption, allowing the integration of the compressor with the EL. Thus, the MH compressor is composed of two stages: the first uses AB_5 $La_{0.9}Ce_{0.1}Ni_5$ alloy and the second AB_2 Hydralloy-C5. These alloys were obtained from providers in form of powder and stocked in air.

Structural and morphological characterization

The morphology and the composition of the received powders were investigated by SEM acquiring SE images of the loose powders (Figure S2-a, b) and through EDX elemental analysis (Table S2). The $La_{0.9}Ce_{0.1}Ni_5$ was received as a fine powder, with an average particle size lower than 0.8 mm (Figure S1-a). From the EDX results, the composition of the $La_{0.9}Ce_{0.1}Ni_5$ was confirmed. Concerning Hydralloy-C5, the powder has a coarser size, with particle dimensions lower than 2 mm, in agreement with producer declaration (Figure S1-b). The Hydralloy-C5 is a $TiMn_2$-based alloy substituted with Zr, Fe and V [35]. The composition declared by the producer was confirmed through EDX elemental analysis (Table S2) and it results in the composition $Ti_{0.95}Zr_{0.05}Mn_{1.55}V_{0.45}Fe_{0.09}$, in agreement with the literature [36–38].

PXD patterns were acquired to investigate alloy's structure and the possible presence of secondary phases. In both samples, no secondary phases were detected, and their structural information were evaluated through the Rietveld refinement (Figure S3). The $La_{0.9}Ce_{0.1}Ni_5$ (Figure S3-a) has the same $CaCu_5$ structure space group *P6/mmm* of the $LaNi_5$, with cell parameters $a = 4.980(7)$ Å and $c = 3.992(2)$ Å. Because in $LaNi_5$ the cell parameter *a* is equal to 5.01(8) Å and *c* equal to 3.98(7) Å [39], it turned out that the substitution of La with Ce causes a decrease in the cell parameter *a* and a slight increase in the cell parameter *c*, that promotes an increment in the equilibrium pressure as reported in Ref. [40]. The Hydralloy-C5 (Figure S3-b) has the hexagonal phase Laves-(C14) with obtained cell parameters *a* equal to 4.873(3) Å and *c* to 7.988(5) Å.

H_2 sorption properties

Alloys for hydrogen sorption typically require an activation before the first hydrogenation [41], that has to be performed directly on the plant. Both compression stages have been designed to be able to be activated simultaneously in the same conditions of pressure and temperature, to allow an easy plant management. Due to design requirements and safety issues, temperature and pressure in the plant cannot exceed 350 bar and 200 °C, respectively. Therefore, being 150 °C the selected T_{high} in the compression stages, an activation procedure at the same temperature was developed, to avoid changes in temperature between the activation and the compression processes. Both alloys have been activated in isothermal conditions at 150 °C, alternating the loading of H_2 in the alloy at 50 bar and the unloading at 1 bar bar. Six cycles were necessary in total for the complete activation of the $La_{0.9}Ce_{0.1}Ni_5$ and ten for the Hydralloy-C5.

After the activation, pcT-curves were acquired at 25 °C, 42 °C, 65 °C, and 87 °C for the $La_{0.9}Ce_{0.1}Ni_5$ (Fig. 2-a), and at 32 °C, 56 °C and 79 °C for the Hydralloy-C5 (Fig. 2-b).

From experimental data, enthalpy (ΔH) and entropy (ΔS) have been obtained by the Van't Hoff plot, for both hydrogen absorption and desorption reactions (Figure S4). Values were calculated taking the equilibrium pressure in the middle of the plateau per each temperature (0.8H_2 wt.% for the $La_{0.9}Ce_{0.1}Ni_5$ and 1.2H_2 wt.% for the Hydralloy C-5). Table 1 reports obtained thermodynamic parameters, namely $\Delta H_{abs/des}$ and $\Delta S_{abs/des}$.

In both cases, experimental thermodynamic data are in agreement with those reported in the literature, where, for the $La_{0.9}Ce_{0.1}Ni_5$, values of, respectively, ΔH and ΔS in absorption of 26.3 kJ/molH_2 and 100 J/molK and desorption of 31.5 kJ/molH_2 and 113 J/molK are reported in Ref. [42], while for the Hydralloy-C5, 23 kJ/molH_2 and 97 J/molK in absorption and 28 kJ/molH_2 and 112 J/molK in desorption are reported in Ref. [43]. From obtained pcT-curves (Fig. 2a–b), it can be observed that a remarkable hysteresis is present for the $La_{0.9}Ce_{0.1}Ni_5$, while the slope is limited in both alloys, but it increases with increasing temperatures, especially for the Hydralloy-C5 in absorption. Using obtained thermodynamic data, by applying the Van't Hoff equation, the equilibrium pressure in absorption and desorption, P_{low} and P_{high}, were evaluated at the T_{low} of 20 °C and T_{high} of 150 °C, and results are reported in Table 1. As expected by the market survey, the Hydralloy-C5 should release hydrogen at pressure higher than 200 bar, *i.e.* 236 bar, at 150 °C, while the $La_{0.9}Ce_{0.1}Ni_5$ could be directly loaded with hydrogen supplied by the EL, thanks to its low equilibrium pressure of 9 bar at 20 °C. It is worth noting that the Hydralloy-

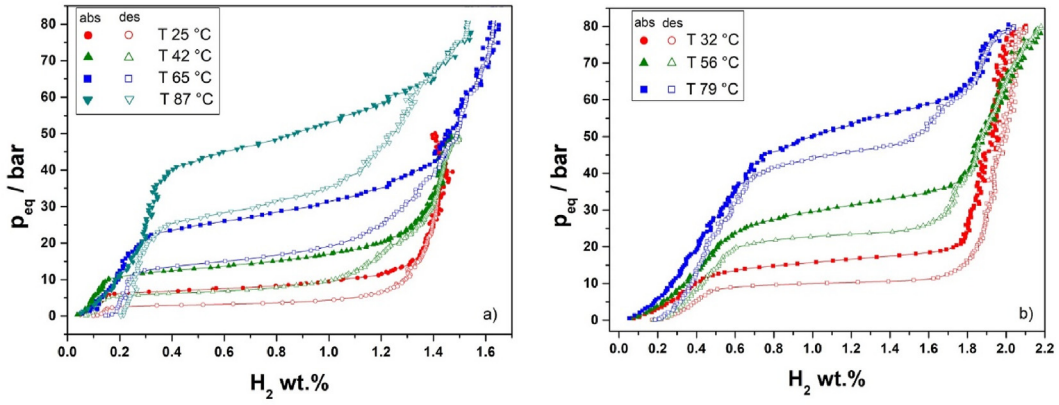

Fig. 2 – pcT-curves in absorption (full points) and desorption (empty points): a) for $La_{0.9}Ce_{0.1}Ni_5$ and b) for Hydralloy-C5.

Table 1 – Experimental $\Delta H_{abs/des}$ and $\Delta S_{abs/des}$ and the equilibrium pressure, P_{low} and P_{high}, calculated at a T_{low} of 20 °C and T_{high} of 150 °C, respectively, for selected alloys.

Alloy	ΔH_{abs} kJ/molH$_2$	ΔS_{abs} J/molK	P_{low} bar	ΔH_{des} kJ/molH$_2$	ΔS_{des} J/molK	P_{high} bar
$La_{0.9}Ce_{0.1}Ni_5$	26	106	9	31	115	150
Hydralloy-C5	23	98	13	29	113	236

C5 shows also a low equilibrium pressure at T_{low}, *i.e.* 13 bar, being able to absorb H_2 directly from the EL, resulting suitable for a single stage MH compressor, if high purity H_2 would be available.

The kinetics of hydrogen loading in $La_{0.9}Ce_{0.1}Ni_5$ was evaluated by performing an absorption curve in working conditions similar to those of the plant, *i.e.* 25 °C and 23 bar. In these conditions, the 90% of the capacity is processed in 10 min, achieving 1.2H_2 wt.%, while the maximum amount of about 1.4H_2 wt.% was reached in 20 min.

Development of the hydrogen refuelling station

MH-reactors

The amount of IMC to allocate inside the reactors was calculated considering compressing hydrogen at 236 bar (the equilibrium pressure of the Hydralloy-C5 at 150 °C, Table 1) in about 5 h, to guarantee one charge per day of the 3.0 l cylinder. Moreover, it was necessary to consider that the same amount of H_2 has to be absorbed at both stages, but selected alloys have different H_2 storage capacity, *i.e.* 1.2H_2 wt. % for the $La_{0.9}Ce_{0.1}Ni_5$ and 1.6H_2 wt.% for the Hydralloy-C5 (deduced from the pcT-curve at 32 °C of Fig. 2-b). It resulted in the use of a lower amount of Hydralloy-C5 in the second stage (700 g) compared to the first one (880 g) of $La_{0.9}Ce_{0.1}Ni_5$.

Reactors were made in AISI 316 stainless steel, with a double tube geometry and with the same volume. Dimensions were evaluated for the first reactor (R1), that was designed considering leaving 30% of free volume to allow the expansion of the alloy during hydrogen absorption. Since the second reactor (R2) has the same dimension of R1, but a lower amount of powder, it resulted in almost a 50% of free volume. Table 2 reports dimensions of R1 and R2. Fig. 3 shows the design of one reactor through a CAD representation, describing the evolution of successive layers, from the powder (i) to the final reactor (iv).

Table 2 – Reactor's dimensions.

Internal diameter ($Ø_{int}$) porous metallic filter	12 mm
Porosity of the metallic porous filter	0.2 μm
Reactor length	389 mm
Internal reactor volume	0.363 dm^3
Øint inner tube	42.2 mm
Øint outer tube	52 mm
Thickness	4.85 mm
$Ø_{int}$ capillary for the heat exchange	3 mm

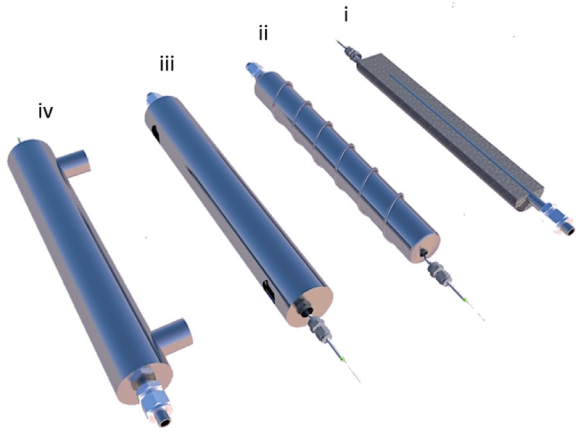

Fig. 3 – Details of the design of the MH-reactor with a CAD highlighting: i) the powder with inside the porous filter for the flow of H_2, ii) the external part of the inner tube with the capillary, iii) and iv) the external jacket and coating.

The IMC was inserted as loose powder in the inner tube of the reactor (Fig. 3-i). Inside the reactor, a homemade porous metallic filter is located to allow a homogeneous distribution of the H_2 in the powder-bed. The filter consists of a tube in steel

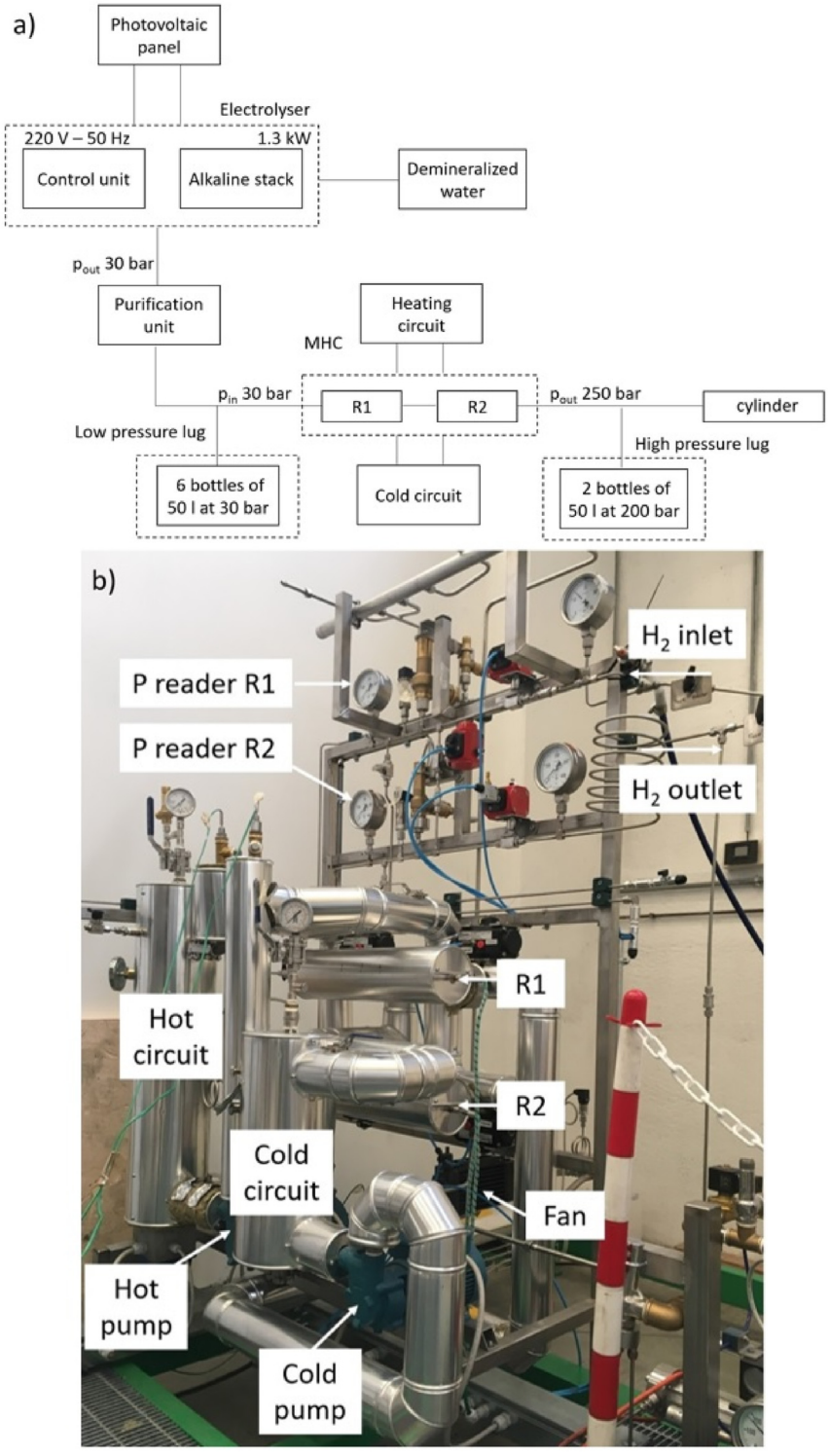

Fig. 4 – a) PFD of the H2RS; b) detailed picture of the MH compressor.

with holes on the surface, coated with a metallic sheet with 2 μm porosity (Table 2). The filter helps also to prevent the spread of the powder out from the reactor. The gas inlet and outlet occur from the same filter. At the connection of the reactor with the hydrogen line, an additional filter of 0.5 μm is present to assure that the powder is not spread along the gas line. In the double tube geometry, the external jacket is dedicated to the flow of the thermal fluid that is forced thanks to a small metallic capillary (Fig. 3-ii-iv). Finally, the reactor was insulated with rock-wool and closed in an aluminium coating.

System integration

Fig. 4-a shows the Process Flow Diagram (PFD) of the realized H2RS.

A control panel allows the opening/close of the pneumatic valves of the H_2 and thermal fluid lines and the switching on/

off of the components of the thermal circuit. The hydrogen line was realized entirely using tubes in AISI 316L stainless steel, with an external diameter of 6 mm and a thickness of 1.5 mm. At the stack of the EL, H_2 was produced at 42 °C with a pressure of 32 bar. As can be seen from the PFD (Fig. 4-a), downstream of the purification unit a bundle of 6 cylinders of 50 l is present, which was filled with the H_2 produced by the EL. It is a low-pressure storage to guarantee a hydrogen buffer to assure the operability of the H2RS in case of stop of the H_2 production through electrolysis. Then as can be seen from Fig. 4-a, at the outer of the compression unit, a high-pressure storage of 2 cylinders of 50 l up to 200 bar is also present to assure a fast high-pressure refuelling, when necessary (Fig. 4-a). At the outlet of the purification stage, H_2 flows towards the bundle and to the compressor. A detailed picture of the compressor is shown in Fig. 4-b. MH-reactors are located horizontally to avoid tension on reactor walls [44]. Temperature and pressure are registered as a function of time during absorption/desorption steps. A three-points thermocouple is located inside the MH-bed, while digital and analogical pressure readers are present along the H_2 line. Thermocouples are also located at the input and output of the two-thermal circuits. The two thermal circuits are separated (Fig. 4) and the design of the thermal management allows that, while one reactor is warmed (*i.e.* desorption stage), the other is cooled (*i.e.* absorption stage), but it is also possible to heat/cool both reactors in parallel, as necessary during the activation process, to allow the simultaneous processing of the alloys. As thermal fluid, the oil Therminol was used, that flows thanks to pumps, one per each circuit. In the hot circuit, the oil is warmed up by an electrical resistance regulated by a thermostat, while in the cold one, it is cooled using a fan. The H_2 at the outlet of the MH compressor can be directly stored in the 3.0 l cylinder.

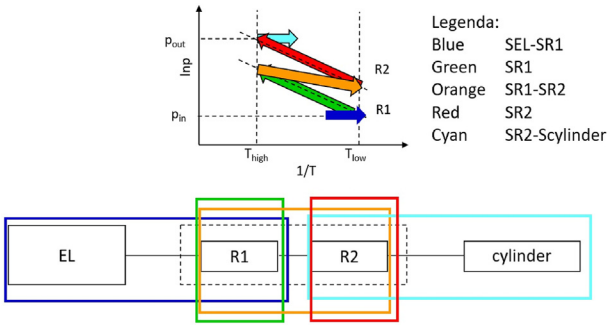

Fig. 5 – Schematic representation of one cycle of compression through a Van't Hoff plot and the connection between EL, R1, R2 and the cylinder, using different segments and colours as link between the two representations identifying different steps of compression. In legenda the names assigned at the various coloured steps are reported. (For interpretation of the references to color in this figure legend, the reader is referred to the Web version of this article.)

Hydrogen compression

One cycle of hydrogen compression is schematically explained in Fig. 5, with a Van't Hoff plot showing various steps and the connection with EL, R1, R2 and the cylinder. Tests were performed filling the 3.0 l cylinder, but also 0.5 l and 1.1 l cylinders were considered, to evaluate the influence of the final volume on the H_2 flow.

One compression cycle starts with the absorption of H_2 by the alloy in R1 directly from the EL at the T_{low} (step named SEL-SR1). When the absorption is completed, the connection with the EL is closed, and R1 is heated at T_{high} (step named SR1), with H_2 increasing the pressure. Then, H_2 is transferred from R1 to R2, which is at T_{low} (step named SR1-SR2). R2 receives continuously H_2 released by R1 at T_{high} at a pressure higher than that necessary for absorption in R2 at T_{low}. When the transfer of H_2 is finished and the MH in R2 is formed, the valve between R1 and R2 is closed and R1 is cooled down to T_{low}, while R2 is heated up to T_{high} (step named SR2). As occurred in SR1, in SR2 the heating of the MH implies the release of H_2 at high pressure, and when R2 is in connection with the cylinder (step named SR2-Scylinder), the H_2 desorbed by the alloy in R2 is directly transferred into the cylinder, filling it.

A fast absorption is observed by the Hydralloy-C5 in R2, when absorbing hydrogen from the $La_{0.9}Ce_{0.1}Ni_5$ in R1, promoted by the high difference in pressure between the desorption pressure of the $La_{0.9}Ce_{0.1}Ni_5$ at 150 °C, i.e. 130 bar, and the equilibrium pressure in absorption of the Hydralloy-C5 at room temperature, *i.e.* 13 bar (Table 1). Indeed, the rate of the hydrogen absorption reaction can be described by a first order equation [45], in which, the reaction rate (v) is directly proportional to the difference between the operative pressure (p) and the equilibrium one (p_{eq}), representing one of the main driving forces of the reaction ($v = k\ (p\text{-}p_{eq})$, where k is the reaction rate constant). Thus, the higher is the difference between the supply and the equilibrium pressure, the higher would be the expected reaction rate.

Fig. 6 shows the variation in temperature and pressure registered during one cycle of compression in a 3.0 l cylinder, named, for the pressure, as pR1 and pR2 and, for the temperature, as TR1 and TR2, in R1 and R2, respectively. The various steps in the compression cycle, as shown in Fig. 4, are identified by five zones with different colours. The cycle refers to an intermediate cycle, in which there is already some H_2 in the gas line left from the previous one.

The various steps are briefly described here below.

SEL-SR1: as reported in Fig. 5, and as can be visualized in Fig. 6, the H_2 is absorbed by the $La_{0.9}Ce_{0.1}Ni_5$ in R1 at a constant pressure of 30 bar (pR1) supplied by the EL, at T_{low}. The latter depends on the temperature of the room, that was about 30 °C during the test, as can be seen from the value TR1 and TR2 at the beginning of the plot. The hydrogen absorption causes a sharp increase in temperature of the powder-bed in R1 (TR1), linked to MH formation, that is an exothermic reaction. In the last part of reaction, a lower amount of H_2 is absorbed, so the heat generated from the reaction decreases and TR1 progressively decreases, moving back to the initial value of about 30 °C, driven by the thermal fluid. Being the connection between EL and R1 always open, pR1 remains constant at about 30 bar.

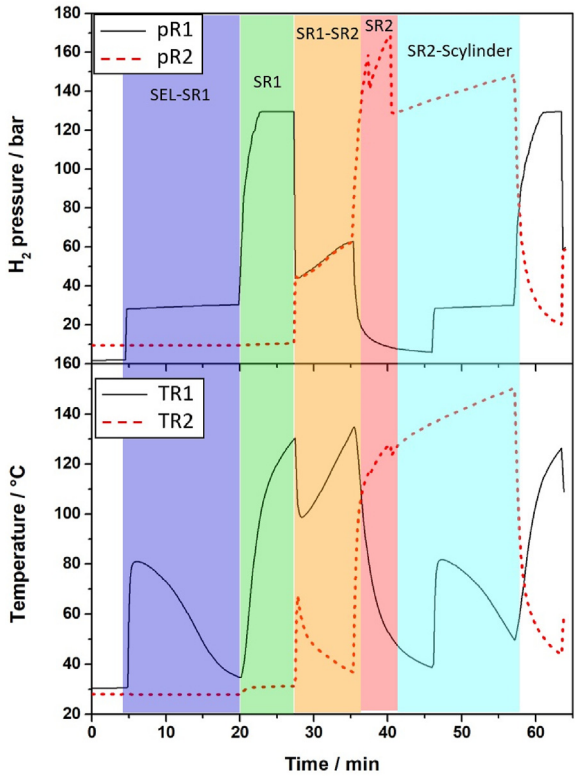

Fig. 6 – The H_2 pressure and temperature for R1 (black continuous lines) and R2 (red dashed lines) as a function of time, reported for one cycle of compression. The various steps, as reported in Fig. 4, are identified by colours (steps that occur before/after the one compression cycle are not coloured). (For interpretation of the references to color in this figure legend, the reader is referred to the Web version of this article.)

SR1: the connection with the EL is closed and R1 is warmed up at the T_{high} (TR1). pR1 achieved a stable value of 130 bar, while heating the reactor up to a maximum value of 130 °C, as can be seen following TR1. Thus, the achievement of the 150 °C, planned T_{high}, is not necessary. Thus, when a stable value for pR1 is reached, the connection between R1 and R2 can be opened (SR1-SR2).

SR1-SR2: TR1 decreases down to 100 °C, while TR2 increases up to about 70 °C, and the pressure of the two reactors reaches a common value. As soon as the connection is opened, the H_2 released by the $La_{0.9}Ce_{0.1}Ni_5$ in R1 is simultaneously absorbed by the Hydralloy-C5 in R2, promoting the local cooling of the MH bed in R1 since the process is endothermic (TR1 decreasing) and a local warming in R2 because of the exothermicity of absorption reaction (TR2 increasing). As the reaction proceed, both pR1 and pR2 maintain the same value and a progressive increase of internal pressure of the system is observed. In the meantime, TR1 moves back toward higher values driven by thermal fluid, and, similarly, TR2 is driven back to 30 °C.

SR2: at the end of the hydrogenation of the Hydralloy-C5, the connection between R1 and R2 is closed, and the circuits of the thermal fluid are swapped, so that R1 is cooled down to T_{low} and R2 is heated up to T_{high}. In R1, the cooling causes a reduction of the pressure and the progressive absorption of the free hydrogen left at the end of the previous step. In the meantime, the rise of TR2 leads to an increase of pR2, as expected.

Table 3 – Time per step of a compression cycle in test 1 and 2.

	SEL-SR1	SR1	SR1-SR2	SR2	SR2-Scylinder
Test 1	10–15 min	5 min	2–5 min	15 min	5 min
Test 2	10–15 min	5 min	2–10 min	5 min	15 min

SR2-Scylinder: finally, the connection between R2 and the cylinder is opened. As can be seen in Fig. 6, there is a drop in TR2, due to the endothermicity of the desorption reaction in R2, as already mentioned for R1 in SR1-SR2. Also, pR2 has a drop due to the filling of the cylinder, and then it increases, thanks to the continuous desorption of H_2 from the Hydralloy-C5. pR2 refers also to the pressure of the cylinder, since, as occurred when the two reactors were connected (SR1-SR2), when connecting R2 with the cylinder, the pressure is equilibrated. When the connection between R2 and the cylinder is interrupted (min 58), the compression cycle is finished and the temperature in R2 is brought again to T_{low}. Thanks to the design of the thermal circuit, *i.e.* to the fact that while one stage is warmed the other is cooled, it is possible to start a new compression cycle in the last 10 min of desorption from the Hydralloy-C5 in R2. Indeed, when R1 reaches the T_{low} (min 46) a new absorption cycle started again (rise in TR1).

As can be seen in Fig. 6, following the increase of TR2 in desorption, the heating rate to reach 150 °C is quite slow, requiring about 20 min. The heat released/absorbed during the hydrogen sorption reactions is observed as a temperature decrease/increase of the MH powder bed and it is an indication of the amount of hydrogen exchanged in the specific stage. Indeed, the higher is the variation in temperature, the higher is the amount of gas exchanged.

Optimization of compression

In order to define the best working conditions allowing to reach a pressure as high as possible in the shortest time,

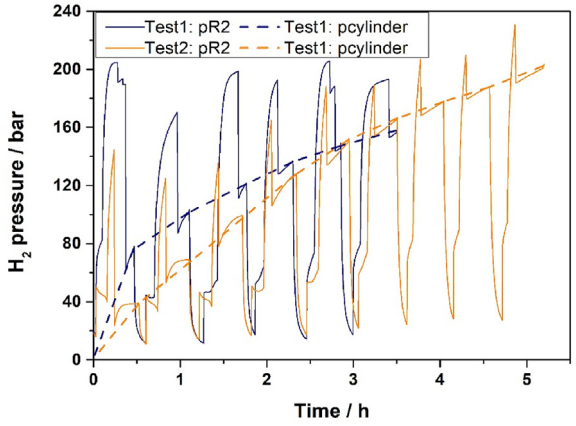

Fig. 7 – Hydrogen pressure of R2 (pR2) as a function of time observed in two tests (solid lines). Dashed lines refer to the progressive charging of the 3.0 l cylinder.

several filling tests were performed. As an example, timing per step for two tests are reported in Table 3. Tests were performed filling a 3.0 l cylinder totally empty, and the difference between the two processes is linked to the time left in the various steps (Table 3).

Fig. 7 shows, as a function of time, pR2 acquired in the two tests (solid lines), together with the pressure reached into the 3.0 l cylinder during filled (dashed lines). Indeed, dashed lines in Fig. 7 connect the pR2 values registered in R2 at the end of each compression cycle, representing the variation of pressure inside the 3.0 l cylinder during the tests of charging.

For the step SEL-SR1, there is no difference in time in the two tests (*i.e.* 10-15 min, Table 3), since it is linked to the reaction time observed for the $La_{0.9}Ce_{0.1}Ni_5$ when testing its absorption reaction rate (Structural and morphological characterization). Considering the temperature profile registered inside the reactor (Fig. 6), the temperature of the room never exceeded 32 °C, implying for absorption a temperature of the powder bed 40 °C < T_{low} < 45 °C, that was the minimum temperature at which the fan was able to cool down the reactor from the previous desorption stage. Despite the high temperature of the MH-powder, the equilibrium pressure of the $La_{0.9}Ce_{0.1}Ni_5$ is still lower than the supply pressure, *i.e.* 25 - 30 bar (Fig. 2-a). Even in the worst absorption conditions, *i.e.* 45 °C and 25 bar, it was not necessary to exceed 15 min. Considering SR1, 5 min are fixed in both tests, since, as previously explained, a stable value of releasing pressure is achieved (Fig. 6). While a different time was investigated in the two tests for SR2, SR1 – SR2 and SR2 – Scylinder.

In test 1, SR1 – SR2 connection time was increased from 2 to 5 min during the loading of the cylinder, followed by a fix time of 15 min for SR2 and a final connection time between R2 and cylinder (SR2-Scylinder) of 5 min. Since 20 min are required to warm up R2 up to 150 °C (Fig. 6), the overall time of SR2 and SR2-Scylinder should not be lower than 20 min, if a high pressure is desired to be reached, in agreement with the thermodynamic study performed on the Hydralloy-C5 (Table 1). In this test, the desorption of the hydrogen was promoted inside the reactor, minimizing the connection with the downstream step, *i.e.* longer time for SR1 and SR2 compared to SR1-SR2 and SR2-Scylinder. It results in an observed charging pressure of the cylinder, *i.e.* the dashed line in Fig. 7, that moves towards a plateau of about 150 bar.

In the second test, it was decided to increase the connection time with the downstream step, *i.e.* SR1-SR2 with 2–10 min and SR2–Scylinder with 15 min, despite of only 5 min for SR2 (Table 3). This strategy should imply the promotion of the absorption of the Hydralloy-C5 during SR1–SR2 and the release of H_2 in the cylinder in the SR2-Scylinder. Indeed, the hydrogen flow moves from a high pressure to a lower one, reaching an equilibrium, as expected when two volumes of gas are put in communication. However, in this case, the equilibrium is driven by the amount of hydrogen that the Hydralloy-C5 can release inside the 3.0 l cylinder. This strategy promotes a constant increase of the charging pressure inside the 3.0 l cylinder, as can be seen following the dashed line in Fig. 7. At the initial stages, the charging pressure is lower compared to test 1, but the pressure increases without reaching a plateau, allowing to achieve 200 bar of charge.

As a conclusion, test 2 resulted to be the best methodology that can satisfy the goal of a high charging pressure of the cylinder. The average time of one cycle of compression was about 47 min in both tests. Nevertheless, test 2 turned out more suitable for the filling of the 3.0 l cylinder up to 200 bar, thanks to a higher connection time in SR1-SR2 and SR2-Scylinder, that allowed the Hydralloy-C5, respectively, to absorb and desorb more H_2.

Hydrogen flow

From Fig. 7, it is possible to observe that the hydrogen pressure in SR2 always reached 200 bar, rising even up 250 bar (peaks in pressure in Fig. 7), which is more than 236 bar expected from thermodynamic parameters (Table 1). As already observed by acquiring the pcT-curves (Fig. 2-b), the latter pressure can be linked to an increase of the slope of the plateau with temperature, allowing to reach a pressure higher than expected from the Van't Hoff equation. On the other hand, the gas remained in the free volume of the reactor contributed to the compression, increasing the overall pressure observed in this stage. The duration of the SR1-SR2 (Table 3) depends on the amount of H_2 desorbed by the Hydralloy-C5 during the charging of the cylinder. Indeed, in first cycles, the low pressure inside the 3.0 l cylinder promotes the desorption of H_2 from the Hydralloy-C5, that, therefore, in the following compression cycles, required a longer time to be completely charged during the absorption from the $La_{0.9}Ce_{0.1}Ni_5$ in

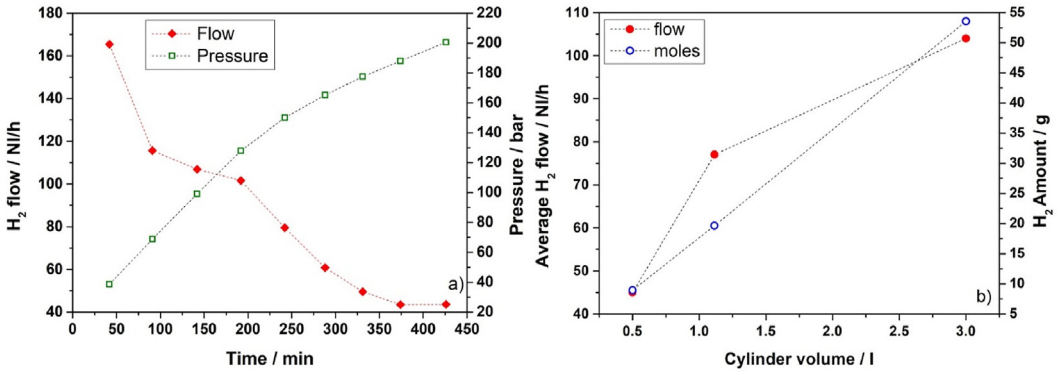

Fig. 8 – a) Hydrogen flow and the charge pressure of the 3.0 l cylinder as a function of the time of charge; b) average hydrogen flow and the compressed amount of H_2 as a function of the volume the cylinder.

SR1–SR2. Afterwards, while the amount of H_2, as well as the pressure, inside the 3.0 l cylinder increased, the Hydralloy-C5 desorbed less and less hydrogen, and a shorter absorption time was required for the SR1–SR2. It resulted in a variable hydrogen flow as can be seen in Fig. 8-a, which reports the H_2 flow and the charge pressure of the 3.0 l cylinder as a function of time. The flow was calculated from the amount of H_2 added in each compression cycle over the duration of it. In Figure S5 the flow and pressure cycle by cycle are reported for the filling of the cylinder of 0.5 and 1.1 l.

Increasing the number of cycles, the flow of H_2 decreases moving towards a plateau, passing from 165 Nl/h to 42 Nl/h and resulting in an average flow of 85 Nl/h. Nevertheless, the design of the system allowed to start a compression cycle in the final 10 min of the previous one, as previously described in Optimization of compression, decreasing the overall time for filling the cylinder. It means that, instead of 426 min required considering the sum of times necessary for each cycle, 374 min were effectively necessary to fill the 3.0 l cylinder, resulting in an effective average flow of 104 Nl/h instead of 85 Nl/h. The same behaviour can be observed for the charging pressure of the cylinder, that has a starting linear increase up to 130 bar, and progressively decreases with the reduction of the flow. This result highlights that the driving force of the process is the difference in content of hydrogen and, in turn, in pressure, between the hydrogen inside the cylinder and the effective amount of H_2 discharged from the Hydralloy-C5, that is linked to its equilibrium pressure at the T_{high}. As far as this difference is high, the desorption from the Hydralloy-C5 is fast. Afterwards, continuing the compression, *i.e.* rising the charged pressure, and so the quantity of H_2, inside the cylinder, the amount of hydrogen released by the Hydralloy-C5 decreased, as well as the desorption rate.

To evaluate the variation of the H_2 flow according to the volume of the cylinder, tests on filling were also carried out with 1.1 l and 0.5 l cylinders. The average flow and pressure trends as a function of the filling time is similar to that described in Fig. 8-a for the 3.0 l cylinder. The same occurs for the temperature and pressure profiles of Fig. 6, and so they are not reported here. Fig. 8-b shows the average H_2 flow as a function of the volume of the filling cylinder (3.0 l, 1.1 l and 0.5 l), and Table 4 reports corresponding values, together with the maximum H_2 flow, *i.e.* the flow in the first cycle of compression, and the maximum final loaded pressure.

For the 1.1 l cylinder, the final charge pressure was 206 bar, having an average flow of 77 Nl/h, while for the 0.5 l, 212 bar was achieved with 45 Nl/h flow observed, (Table 4, Fig. 8-b). Applying the same filling strategy developed for the 3.0 l cylinder (test 2), the average duration of whole compression cycle was equal to 44 min and 42 min for the 1.1 l and 0.5 l, respectively. As it can be seen from Table 4, the maximum hydrogen flow registered in the first cycle of compression for 1.1 l and 3.0 l was the same, *i.e.* 165 Nl/h, to be compared with 105 Nl/h observed for the 0.5 l. 165 Nl/h was attributable to a gravimetric capacity of $La_{0.9}Ce_{0.1}Ni_5$ alloy in R1 of about 1.2H_2 wt.%, in line with the preliminary test (Structural and morphological characterization). Indeed, independently from the filling volume, considering an average time of cycle and excluding the amount of free volume per stage, a flow of H_2 of about 161 Nl/h can be estimated, which is not far from the observed value of 165 Nl/h, where also the free volume in the gas line contributed to the final flow. This means that, in the first cycle, with the cylinder of 3.0 l and 1.1 l, it is possible to promote the discharge of the maximum amount of H_2 available from the MH compressor. On the contrary, with a cylinder of 0.5 l, the volume is not sufficient to optimize the compression process. Fig. 8-b shows the quantity compressed hydrogen as a function of the volume of the cylinder, together with the average flow. As it can be seen, the flow increases increasing the volume of the cylinder, but not linearly. While a linear trend is observed regarding the amount of hydrogen, meaning that the greater the volume of the cylinder the greater is the desorption by the Hydralloy-C5 per cycle, as explained previously with respect to the driving force of the process. Comparing the average flow with the flow registered in the first cycle, for the 3.0 l and 1.1 l cylinder, it represents the 63% and 47% of the maximum one of 165 Nl/h, while for the 0.5 l cylinder, it is the 43% of the maximum observed of 105 Nl/h, and it is only the 27% of the maximum potential of the MH compressor (165 Nl/h).

The maximum pressure reached in step R1 is 130 bar at 130 °C, and it is higher than the value of 100 bar expected from thermodynamic parameters of the $La_{0.9}Ce_{0.1}Ni_5$ alloy at the same temperature. This increase can be associated again to the slope of the plateau in the pcT-curve at 130 °C, and the compression of the free gas left inside the reactor post-absorption, as already mentioned for R2, with a maximum pressure of 250 bar at 150 °C. These pressure values were found during desorption in reactor not connected with the downstream volumes (SR1 and SR2). The supply pressure for the R1 considering the connection with the EL had an average of 28 bar with a minimum down to 25 bar and resulting in a compression ratio, CR, (desorption pressure in R2 over the supply pressure in R1) equal to 9 and 10, respectively. Taking into account that from a thermodynamic point of view, the $La_{0.9}Ce_{0.1}Ni_5$ alloy could absorb H_2 at even lower pressure (Table 1), the supply pressure might be even decreased, in favour of an increase in CR.

Table 4 – Maximum hydrogen flow, average flow and maximum loading pressure related to different volumes of the cylinder.

Cylinder volume l	Maximum flow Nl/h	Average flow Nl/h	Load pressure bar
3.0	165	104	200
1.1	165	77	206
0.5	105	45	212

Thermal fluid

In order to evaluate the flow of the thermal fluids, the temperature and pressure were monitored, per each circuit, at the inlet and outlet of reactors. The volumetric flow remained constant during operations of the MH compressor, and it was equal to 1.0 m^3/h for the hot circuit and 0.8 m^3/h for the cold one.

Fig. 9 shows, for one cycle of compression, the temperature profiles of the thermal fluids, as called $T_{in/out}$ Hot, for the hot circuit, and $T_{in/out}$ Cold, for the cold one. The single

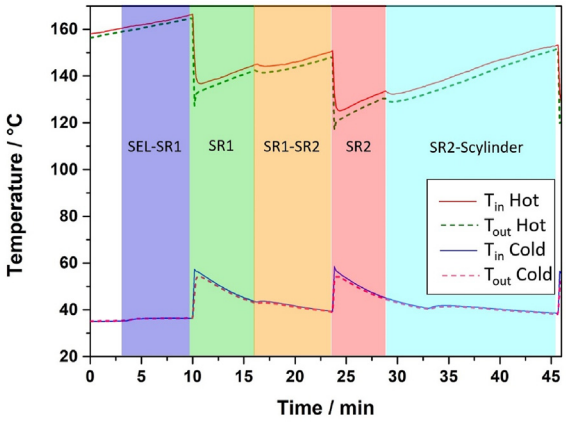

Fig. 9 – Thermal fluid temperature inlet and outlet registered at the hot and cold circuit during one cycle of compression. Colours are used to distinguish various compression steps as reported in Fig. 6. (For interpretation of the references to color in this figure legend, the reader is referred to the Web version of this article.)

compression steps are highlighted as for Fig. 6, through the coloured zones.

Looking at the temperature of the thermal fluid in the cold circuit, when the hydrogen is absorbed by the $La_{0.9}Ce_{0.1}Ni_5$ alloy in R1, *i.e.* SEL-SR1, and by the Hydralloy-C5 alloy in R2, *i.e.* SR1–SR2, there was an increase in temperature of about 1.0 °C, due to the exothermic absorption process, with a difference between inlet and outlet of 0.5 °C. This means that, while locally inside the MH-powder there was a substantial increase in temperature of about 20–30 °C, as observed in Fig. 6, the system at macroscopic scale was not warmed up. Indeed, the role of the cold thermal circuit in absorption is to avoid the warming up of the entire system due to the exothermicity of the reaction. In this case, the thermal fluid is efficiently removing most of the heat generated, since only 0.5 °C are attributed to the warming up of the system because of the absorption reaction. The same can be observed in desorption, considering the hot thermal fluid. In this case, to contrast the decrease in temperature promoted by the endothermicity, visible at local level inside the MH-power (Fig. 6), when the $La_{0.9}Ce_{0.1}Ni_5$ alloy was desorbing in SR1-SR2, and the Hydralloy-C5 alloy in SR2-Scylinder, the thermal fluid needed to efficiently release heat to avoid the cooling down of the system. In this case, the difference between inlet and outlet temperature was always approximately of 2.0 °C, with a decrease due to the reaction of 2.0 °C. The hot thermal fluid reached a maximum temperature of 165 °C to guarantee a powder temperature in R2 of 150 °C. When the circuit needed to be swapped, *i.e.* from cold to hot and vice versa, it was always observed an increase in temperature of the cold fluid of about 30 °C and a decrease in the hot one of approximately the same amount. These stages occurred in SR1 and SR2, that refer to the change from absorption to desorption.

Power, energy and isentropic efficiency

The power consumed by the MH compressor was calculated to investigate the feasibility of the MH compressor in real applications. Moreover, the evaluation of the power necessary is also fundamental to understand a possible optimization of the design thinking for an up-scaling of the system. The amount of power required by the MH compressor (P_{MHC}) was calculated according to Equation (1):

$$P_{MHC} = P_{dissipated} + P_{abs} + P_{des} + P_{pumpcold} + P_{pumphot} \quad \text{Eq. (1)}$$

where $P_{dissipated}$ is the total power dissipated given by the sum of the power dissipated by the non-insulated surfaces (hot pump, handwheels of the thermal circuit, brass components of the hot circuit in which the thermocouples are located), by the pipes and by the tank of the hot circuit. Then, P_{abs} and P_{des} are, respectively, related to absorption and desorption, taking into account the power to cool/heat the MH powder, the reactor and the reaction enthalpy, considering the filling of the 3.0 l cylinder. Finally, $P_{pumpcold}$ and $P_{pumphot}$ refer to the power necessary to the pump in the cold and hot thermal circuit, respectively, for the flow of the thermal fluid to keep the temperature of the system.

The $P_{dissipated}$ turned out equal to 201 W, $P_{pumpcold}$ and $P_{pumphot}$ was equal to 164 W for each pump, while the values related to the reaction of hydrogen, *i.e.* P_{abs} and P_{des}, were 39 and 46 W, respectively. Thus, the amount of power consumed by the compressor (P_{MHC}) to compress the hydrogen, filling the 3.0 l cylinder, is 614 W for less than 1 kg of MH in each reactor. Nevertheless, most of the contribution are related to the plant, $P_{pumpcold}$, $P_{pumphot}$ and $P_{dissipated}$, instead of the reaction itself, P_{abs} and P_{des}, highlighting that a better insulation is mandatory to promote a reduction of the power required by the system.

The energy required to start-up of the entire plant was calculated considering the energy necessary to heat the plant from room temperature to 150 °C. Calculations took into account the energy to heat up the pump, the tank, the thermal fluid, the pipes and the reactor. The overall amount of energy required to turn on the plant was estimated equal to 1.0 kWh, suggesting that in less to 2 h the compressor is able to reach the steady state conditions.

Finally, the isentropic efficiency (η), that represents the ratio between the isentropic work of compression (W) and the energy used for compression (Q), was evaluated according to Eqs. (2)–(4) [46]:

$$\eta = \frac{W}{Q} \quad \text{Eq. (2)}$$

with

$$W = \frac{\gamma}{\gamma - 1} m_{H2} T_{abs} \left[\frac{R}{M_{H2}}\right] \left[\left(\frac{P_{des}}{P_{supp}}\right)^{\frac{\gamma-1}{\gamma}} - 1\right] \quad \text{Eq. (3)}$$

$$Q = n\Delta H_{des} + \left(C_{steel} m_{steel} + C_{alloy} m_{alloy}\right)\left(T_{des} - T_{abs}\right) \quad \text{Eq (4)}$$

where γ is the isentropic coefficient, C is the specific heat, R is the gas constant, m is the mass, M the molecular mass, P is the pressure and T temperature, while the abs/des subscripts stand for absorption/desorption and supp for supply. Considering the filling of the 3.0 l cylinder, a W of 215 kJ and a Q of 1876 kJ, resulting in an isentropic efficiency η of 11% for a compression ratio of 9. While 12% is obtained with a compression ratio of 10, implying that the efficiency is higher

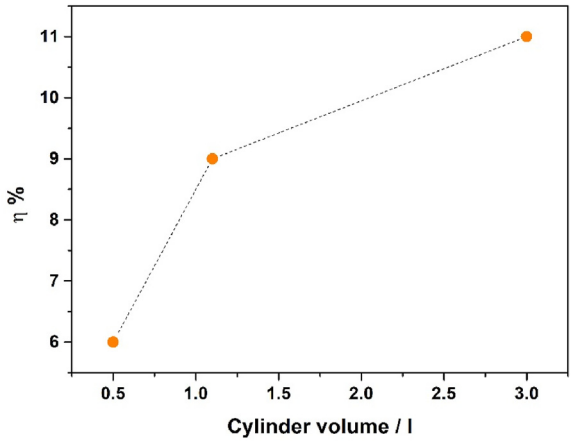

Fig. 10 – Isentropic efficiency in percentage as a function of the cylinder volume.

when decreasing the supply pressure, as was already suggested by Muthukumar et al. [47]. Values with up to a maximum of about 20% of efficiency have been reported in the literature [46–48]. However, it is important to point out that the used methodologies to evaluate the efficiency are not unique, and different equations, data from simulations or models can be used. In this case, the overall amount of gas compressed by the plant was considered, according to the methodology reported in Ref. [46].

Considering other volumes of cylinders, with a compression ratio of 9, it was possible to observe a progressively increase in η, increasing the volume, but not linearly, as can be observed in Fig. 10.

This trend is linked to the amount of hydrogen processed, highlighting that the 0.5 l volume is not suitable for the developed system, while 3.0 l represents a proper filling volume, observing the highest amount of hydrogen compressed and isentropic efficiency. This result confirms that the system was properly sized during the design of the MH compressor (MH-reactors).

Alloys' characterization after their operation inside the MHC

The MH compressor performed 352 compression cycles, resulting in an average working time of about 245 h, without detecting significant losses in performances. Few grams of alloys were taken out from the reactors after the tests and characterized.

The cycling in hydrogen promoted a sensitive reduction of the particle size, thanks to the variation in crystalline cell volume between the hydride and the compounds in absorption and desorption [41], as it was investigating by acquiring SEM–SE images. Considering the $La_{0.9}Ce_{0.1}Ni_5$ powder, the average particle size passed from below 0.8 mm (Figure S1-a) to below 25 μm after the cycling in plant (Figure S1-c). On the other hand, in the Hydralloy-C5 powder, a most homogenous dimension of less than 150 μm (Figure S1-d) was observed compared to a coarse particle size of less than 2 mm (Figure S1-b). The chemical composition of the alloys was investigated by EDX. Concerning the $La_{0.9}Ce_{0.1}Ni_5$ alloy, when the matrix was detected, it was observed that the starting composition was maintained, while some Ni and La rich in oxygen were also detected. These results suggest the occurrence of a disproportion reaction, that was also confirmed by acquiring the PXD pattern (Figure S6-a). Together with the diffraction peaks of the main phase, those related to Ni (fcc) and to an unknown phase are highlighted in the pattern, with black continuous line and dots, respectively (Figure S6-a). The proper stoichiometry of the unknown phase is hard to assign due to background noise and the amorphous band at low angles related to the capillary. From the qualitative analysis of the PXD pattern, the unknown phase is not related to the LaH_2 (phase expected from the disproportion of $LaNi_5$-based alloys [44,49]), but likely to an La-oxide, like La_2O_3, or a La-hydroxide phase, like $La(OH)_3$. Indeed, in the literature, it is reported the occurrence of a disproportion in $LaNi_5$-alloys in presence of oxygen resulting in the formation of $La(OH)_3$, La_2O_3 and Ni particles [50]. In this work, the hydrogen absorption in $La_{0.9}Ce_{0.1}Ni_5$ alloy acts as a purification stage for hydrogen to be provided to the Hydralloy-C5 alloy. So, the occurrence of oxidation in R1could be linked to the impurities of oxygen/water present in the hydrogen supply flow coming from the EL. In addition, it has to be considered that the removal of the alloys from the reactor occurred not in a proper inert atmosphere and after several months after the final usage in the plant. This might have promoted a possible oxidation too. Concerning the Hydralloy-C5 powder, from the EDX analysis it was observed that the composition of the matrix is maintained, and no degradation or oxidation occurred during cycling. Indeed, by acquiring the PXD pattern, no secondary phases were detected (Figure S6-b). The significant decrease of powder size observed by the SEM–SE images promoted a sensitively increase in the sorption rate, as it was observed by acquiring an absorption curve for the $La_{0.9}Ce_{0.1}Ni_5$ alloy in the same temperature and pressure conditions registered before and after its use in the MH compressor (Figure S7-a). The curve in Figure S7-a named *"Before MHC"* refers to the first hydrogenation cycle after the activation in the laboratory of the as-received powder. As can be seen, a stable value is reached in about 10 min, on the contrary of less than 1 min in the alloys after cycling in the compressor. For the Hydralloy-C5 alloy, the kinetic curve, registered in the same condition applied for the $La_{0.9}Ce_{0.1}Ni_5$ powder, evidences also a fast sorption rate, with about 2 min required to reach a stable hydrogen content (Figure S7-b). The fast kinetics is likely linked to the reduction of the particle size promoted by the continuous cycling, thanks to the increase of the reactive surface area [51]. Nevertheless, for both alloys, the amount of hydrogen absorbed registered is decreased of about 0.3–0.4H_2 wt.% (Figure S6). A decrease in capacity of the $La_{0.9}Ce_{0.1}Ni_5$ alloy can be attributable to the occurrence of disproportion. Indeed, by calculating the capacity absorbed by the alloy in the last cycles of operability in the MH compressor, a value of 1.1H_2 wt.% was obtained compared to 1.2H_2 wt.% observed at the beginning. However, the loss registered at laboratory level is even lower. A loss in hydrogen sorption capacity was detected also for the Hydralloy-C5 alloy, even if the material did not undergo to any degradation/oxidation. A possible explanation might be assigned to the laboratory instrumental setup. Indeed, as reported in Ref. [44], while locating reactor vertically if sample is present as powder with small dimension, the storage capacity

tends to decrease because of internal stress and material self-densification, that decreases the porosity hindering the diffusion of H_2 [44]. Indeed, the diffusion of hydrogen in MH is lower than in the compound [52] and in vertical displacement of reactor a first layer of MH is formed, hindering the progressive hydrogenation of the alloy. The instrument used in this work for the analysis has a long and narrow tube displaced vertically. Thus, because of the fine powder obtained after the cycling in the compressor, when analysing the powder inside the pcT-instrument, the self-densification occurred, registering the loss in capacity linked only to powder morphology.

In conclusion, the cycling in the plant promoted the occurrence of a disproportion of the $La_{0.9}Ce_{0.1}Ni_5$ alloy, due to impurities of oxygen and water in the gas supply. Since this alloy is acting as purification step in the compressor, this result is important for a possible scale-up of the system. Not significant loss in performances were detected in plant management and with the obtained results it is difficult to predict how could go on the degradation of the $La_{0.9}Ce_{0.1}Ni_5$ alloy up to registering significant losses in performance of the MH compressor. This result highlights the importance to remove efficiently the impurities in the gas supply, since, as observed, the properties of Hydralloy-C5 alloy are maintained.

Conclusions

An integrated system that includes a PV plant, an electrolyzer and a two stages MH compressor was described in detail. The MH compressor was realized based on the commercial alloy $La_{0.9}Ce_{0.1}Ni_5$ alloy in the first stage and the Hydralloy-C5 alloy in the second stage. The system compresses hydrogen from 28 bar supplied by an electrolyser up to 250 bar, working between the room temperature of about 30 °C and 150 °C, resulting in a compression ratio of about 9. Furthermore, an average H_2 flow of 104 Nl/h (*i.e.* 0.003 g/s) was observed with an isentropic efficiency of 11% and a limited power consumption of 614 W. As observed, mostly of the power results from plant contribution, *i.e.* the pumps and the dissipated power, while only 85 W are linked to the absorption and desorption reaction of the hydrogen. The principles behind the compression work result in a variable flow of hydrogen that decreased cycle after cycle while filling the cylinder and also in a variable flow by changing the filling volume.

This work highlights the easy design necessary to develop a MH compressor and its integration in a green hydrogen refuelling station. In particular, the feasibility to use commercial metal hydrides to achieve high pressure of hydrogen, *i.e.* 250 bar that is even higher than the MH compressor previously realized based on commercial alloys reported in Ref. [30]. The advantage is the limited amount of power required and the easy scale-up of the entire refuelling station, thanks to the use of commercially available items, *i.e.* PV panels, EL and MH alloys, encouraging its spread in the market.

Future work can be linked to the improvement of MH compressor performances, investigating the influence of the thermal vector flow, the feasibility to use solar panels to generate the heat necessary for the reactions, in order to move towards a fully green hydrogen refuelling station.

Nevertheless, this work points out the limited pressure that can be reached with compounds available on the market, implying a narrow range of applications in the market. There is the need to develop commercially available alloys able to compress hydrogen at higher pressures, for the possible development of H_2 refuelling stations based on MH compressor, where 400 bar or more than 700 bar are required.

Declaration of competing interest

The authors declare that they have no known competing financial interests or personal relationships that could have appeared to influence the work reported in this paper.

Acknowledgement

This publication is part of the project NODES which has received funding from the MUR – M4C2 1.5 of PNRR with grant agreement no. ECS00000036. Authors acknowledge the Regione Piemonte (Italy) for the financial support at the project Clean-DronHy, POR-FESR 2014/2020.

Appendix A. Supplementary data

Supplementary data to this article can be found online at https://doi.org/10.1016/j.ijhydene.2023.05.155.

REFERENCES

[1] Sdanghi G, Maranzana G, Celzard A, Fierro V. Review of the current technologies and performances of hydrogen compression for stationary and automotive applications. Renew Sustain Energy Rev 2019;102:150–70. https://doi.org/10.1016/j.rser.2018.11.028.

[2] Barthélémy H. Hydrogen storage - industrial prospectives. Int J Hydrogen Energy 2012;37:17364–72. https://doi.org/10.1016/j.ijhydene.2012.04.121.

[3] Topler J, Lehmann J. Hydrogen and fuel cell. Springer Berlin Heidelberg; 2016. https://doi.org/10.1007/978-3-662-44972-1.

[4] Lototskyy M, Davids MW, Swanepoel D, Louw G, Klochko Y, Smith F, Haji F, Tolj I, Chidziva S, Pasupathi S, Linkov V. Hydrogen refuelling station with integrated metal hydride compressor: layout features and experience of three-year operation. Int J Hydrogen Energy 2020;45:5415–29. https://doi.org/10.1016/j.ijhydene.2019.05.133.

[5] Jensen JO, Vestbø AP, Li Q, Bjerrum NJ. The energy efficiency of onboard hydrogen storage. J Alloys Compd 2007;446–447:723–8. https://doi.org/10.1016/j.jallcom.2007.04.051.

[6] Nicolas V, Sdanghi G, Mozet K, Schaefer S, Maranzana G, Celzard A, Fierro V. Numerical simulation of a thermally driven hydrogen compressor as a performance optimization tool. Appl Energy 2022;323:119628. https://doi.org/10.1016/j.apenergy.2022.119628.

[7] Pineda-Delgado JL, Chávez-Ramirez AU, Gutierrez B CK, Rivas S, Marisela CR, de Jesús Hernández-Cortes R, Menchaca-Rivera JA, Pérez-Robles JF. Effect of relative humidity and temperature on the performance of an

electrochemical hydrogen compressor. Appl Energy 2022;311. https://doi.org/10.1016/j.apenergy.2022.118617.
[8] Lototskyy MV, Yartys VA, Pollet BG, Bowman RC. Metal hydride hydrogen compressors: a review. Int J Hydrogen Energy 2014;39:5818–51. https://doi.org/10.1016/j.ijhydene.2014.01.158.
[9] Bellosta von Colbe J, Ares J-R, Barale J, Baricco M, Buckley C, Capurso G, Gallandat N, Grant DM, Guzik MN, Jacob I, Jensen EH, Jensen T, Jepsen J, Klassen T, Lototskyy MV, Manickam K, Montone A, Puszkiel J, Sartori S, Sheppard DA, Stuart A, Walker G, Webb CJ, Yang H, Yartys V, Züttel A, Dornheim M. Application of hydrides in hydrogen storage and compression: achievements, outlook and perspectives. Int J Hydrogen Energy 2019;44. https://doi.org/10.1016/j.ijhydene.2019.01.104.
[10] Costamagna M, Barale J, Carbone C, Luetto C, Agostini A, Baricco M, Rizzi P. Environmental and economic assessment of hydrogen compression with the metal hydride technology. Int J Hydrogen Energy 2022;47:10122–36. https://doi.org/10.1016/j.ijhydene.2022.01.098.
[11] Laurencelle F, Dehouche Z, Goyette J, Bose TK. Integrated electrolyser-metal hydride compression system. Int J Hydrogen Energy 2006;31:762–8. https://doi.org/10.1016/j.ijhydene.2005.06.019.
[12] Visaria M, Mudawar I. Experimental investigation and theoretical modeling of dehydriding process in high-pressure metal hydride hydrogen storage systems. Int J Hydrogen Energy 2012;37:5735–49. https://doi.org/10.1016/j.ijhydene.2011.12.140.
[13] Wang X, Liu H, Li H. A 70 MPa hydrogen-compression system using metal hydrides. Int J Hydrogen Energy 2011;36:9079–85. https://doi.org/10.1016/j.ijhydene.2011.04.193.
[14] Solovey VV, Ivanovsky AI, Kolosov VI, Shmal'ko YF. Series of metal hydride high pressure hydrogen compressors. J Alloys Compd 1995;231:903–6. https://doi.org/10.1016/0925-8388(95)01780-1.
[15] Karagiorgis G, Christodoulou CN, von Storch H, Tzamalis G, Deligiannis K, Hadjipetrou D, Odysseos M, Roeb M, Sattler C. Design, development, construction and operation of a novel metal hydride compressor. Int J Hydrogen Energy 2017;42:12364–74. https://doi.org/10.1016/j.ijhydene.2017.03.195.
[16] Sharma R, Kumar EA. A comparative thermodynamic analysis of gas-solid sorption system based on H2-La0.9Ce0.1Ni5/LaNi4.7Al0.3 and NH3-NaBr/MnCl2. Energy Proc 2017;109:48–55. https://doi.org/10.1016/j.egypro.2017.03.047.
[17] Sekhar BS, Muthukumar P. Performance investigation of a single-stage metal hydride heat transformer. Int J Green Energy 2016;13:102–9. https://doi.org/10.1080/15435075.2014.892879.
[18] Madaria Y, Anil Kumar E. Effect of heat transfer enhancement on the performance of metal hydride based hydrogen compressor. Int J Hydrogen Energy 2016;41:3961–73. https://doi.org/10.1016/j.ijhydene.2016.01.011.
[19] Galvis ARE, Leardini F, Ares JR, Cuevas F, Fernandez JF. Experimental behaviour of a three-stage metal hydride hydrogen compressor. J Phys Energy 2020;2. https://doi.org/10.1088/2515-7655/ab869e.
[20] Hu XC, Qi ZG, Yang M, Chen JP. A 38MPa compressor based on metal hydrides. J Shanghai Jiao Tong Univ (Sci) 2012;17:53–7. https://doi.org/10.1007/s12204-012-1229-5.
[21] Wang XH, Bei YY, Song XC, Fang GH, Li SQ, Chen CP, Wang QD. Investigation on high-pressure metal hydride hydrogen compressors. Int J Hydrogen Energy 2007;32:4011–5. https://doi.org/10.1016/j.ijhydene.2007.03.002.
[22] Li H, Wang X, Dong Z, Xu L, Chen C. A study on 70 MPa metal hydride hydrogen compressor. J Alloys Compd 2010;502:503–7. https://doi.org/10.1016/j.jallcom.2010.04.206.
[23] GRZ Technologies website. https://grz-technologies.com. (accessed 30 May 2023).
[24] HYSTORSYS SA website. http://www.hystorsys.no. (accessed 30 May 2023).
[25] Yartys VA, Lototskyy M, Linkov V, Grant D, Stuart A, Eriksen J, Denys R, Bowman RC, Grant D, Stuart A. Metal hydride hydrogen compression : recent advances and future prospects. Appl Phys A 2016;122:1–18. https://doi.org/10.1007/s00339-016-9863-7.
[26] HySa Systems website. http://www.hysasystems.com. (accessed 30 May 2023).
[27] Yartys VA, V Lototskyy M, Linkov V, Pasupathi S, Wafeeq M, Tolj I, Radica G, V Denys R, Eriksen J, Taube K, Bellosta J, Colbe V, Capurso G, Dornheim M, Smith F, Mathebula D, Swanepoel D, Hydride4Mobility ScienceDirect. An EU HORIZON 2020 project on hydrogen powered fuel cell utility vehicles using metal hydrides in hydrogen storage and refuelling systems. Int J Hydrogen Energy 2021:1–14. https://doi.org/10.1016/j.ijhydene.2021.01.190.
[28] Ulleberg Ø, Meyer J, Eriksen J, Norheim A, Gjerløw JC. Hynor Lillestrøm - a renewable hydrogen station & technology test center. In: 20th world hydrog. Energy Conf.; 2014. p. 132–9.
[29] Kelly NA, Girdwood R. Evaluation of a thermally-driven metal-hydride-based hydrogen compressor. Int J Hydrogen Energy 2012;37:10898–916. https://doi.org/10.1016/j.ijhydene.2012.04.088.
[30] Tarasov BP, Bocharnikov MS, Yanenko YB, Fursikov PV, Lototskyy MV. Cycling stability of RNi5(R = La, La+Ce) hydrides during the operation of metal hydride hydrogen compressor. Int J Hydrogen Energy 2018;43:4415–27. https://doi.org/10.1016/j.ijhydene.2018.01.086.
[31] Belmonte N, Staulo S, Fiorot S, Luetto C, Rizzi P, Baricco M. Fuel cell powered octocopter for inspection of mobile cranes: design, cost analysis and environmental impacts. Appl Energy 2018;215:556–65. https://doi.org/10.1016/j.apenergy.2018.02.072.
[32] Boukoberine MN, Zia MF, Benbouzid M, Zhou Z, Donateo T. Hybrid fuel cell powered drones energy management strategy improvement and hydrogen saving using real flight test data. Energy Convers Manag 2021;236:113987. https://doi.org/10.1016/j.enconman.2021.113987.
[33] Lutterotti L, Matthies S, Wenk HR, Schultz AS, Richardson JW. Combined texture and structure analysis of deformed limestone from time-of-flight neutron diffraction spectra. J Appl Phys 1997;81:594–600. https://doi.org/10.1063/1.364220.
[34] Tarasov BP, Bocharnikov MS, Yanenko YB, V Fursikov P. Metal hydride hydrogen compressors for energy storage systems : layout features and results of long-term tests Metal hydride hydrogen compressors for energy storage systems : layout features and results of long-term tests. J Phys Energy 2020;2:024005.
[35] Nayebossadri S, Book D. Development of a high-pressure Ti-Mn based hydrogen storage alloy for hydrogen compression. Renew Energy 2019;143:1010–21. https://doi.org/10.1016/j.renene.2019.05.052.
[36] Herbrig K, Röntzsch L, Pohlmann C, Weißgärber T, Kieback B. Hydrogen storage systems based on hydride-graphite composites: computer simulation and experimental validation. Int J Hydrogen Energy 2013;38:7026–36. https://doi.org/10.1016/j.ijhydene.2013.03.104.
[37] Dieterich M, Pohlmann C, Bürger I, Linder M, Röntzsch L. Long-term cycle stability of metal hydride-graphite composites. Int J Hydrogen Energy 2015;40:16375–82. https://doi.org/10.1016/j.ijhydene.2015.09.013.
[38] Pohlmann C, Röntzsch L, Heubner F, Weißgärber T, Kieback B. Solid-state hydrogen storage in Hydralloy-graphite composites. J Power Sources 2013;231:97–105. https://doi.org/10.1016/j.jpowsour.2012.12.044.
[39] Chartouni D, Meli F, Züttel A, Gross K, Schlapbach L. The influence of cobalt on the electrochemical cycling stability

of LaNi5-based hydride forming alloys. J Alloys Compd 1996;241:160–6. https://doi.org/10.1016/0925-8388(96)02331-6.
[40] Odysseos M, De Rango P, Christodoulou CN, Hlil EK, Steriotis T, Karagiorgis G, Charalambopoulou G, Papapanagiotou T, Ampoumogli A, Psycharis V, Koultoukis E, Fruchart D, Stubos A. The effect of compositional changes on the structural and hydrogen storage properties of (La-Ce)Ni5type intermetallics towards compounds suitable for metal hydride hydrogen compression. J Alloys Compd 2013;580:S268–70. https://doi.org/10.1016/j.jallcom.2013.01.057.
[41] Broon DP. Hydrogen storage materials the characterisation of their storage properties. Springer-Verlag London; 2011.
[42] Romanov IA, Borzenko VI, Kazakov AN. Using the copper-foam for thermal conductivity improvement of La0.9Ce0.1Ni5-alloy bed during interaction with hydrogen. J. Phys. Conf. Ser. 2019;1359:1–6. https://doi.org/10.1088/1742-6596/1359/1/012103.
[43] Capurso G, Schiavo B, Jepsen J, Lozano G, Metz O, Saccone A, De Negri S, von Colbe JMB, Klassen T, Dornheim M. Development of a modular room-temperature hydride storage system for vehicular applications. Appl Phys Mater Sci Process 2016;122. https://doi.org/10.1007/s00339-016-9771-x.
[44] Jensen EH, Dornheim M, Sartori S. Scaling up metal hydrides for real-scale applications: achievements, challenges and outlook. INORGA 2021;9:1–20. https://doi.org/10.3390/inorganics9050037.
[45] Martin M, Gommel C, Borkhart C, Fromm E. Absorption and desorption kinetics of hydrogen storage alloys. J Alloys Compd 1996;238:193–201. https://doi.org/10.1016/0925-8388(96)02217-7.
[46] Bhogilla SS, Niyas H. Design of a hydrogen compressor for hydrogen fueling stations. Int J Hydrogen Energy 2019;44:29329–37. https://doi.org/10.1016/j.ijhydene.2019.02.171.
[47] Muthukumar P, Prakash Maiya M, Srinivasa Murthy S. Performance tests on a thermally operated hydrogen compressor. Int J Hydrogen Energy 2008;33:463–9. https://doi.org/10.1016/j.ijhydene.2007.07.019.
[48] Palumbo M, Urgnani J, Baldissin D, Battezzati L, Baricco M. Calphad : computer coupling of phase diagrams and thermochemistry thermodynamic assessment of the H – La – Ni system. CALPHAD: Comput Coupling Phase Diagrams Thermochem 2009;33:162–9. https://doi.org/10.1016/j.calphad.2008.09.003.
[49] Boonstra A, Lippits GJM, Bernards TNM. Degradation processed in a LaNi5 electrode. J Less Common Met 1989;255:119–31.
[50] Laurencelle F, Dehouche Z, Goyette J. Hydrogen sorption cycling performance of LaNi 4 . 8 Sn 0 . 2. J Alloys Compd 2006;424:266–71. https://doi.org/10.1016/j.jallcom.2005.11.085.
[51] Kazakov AN, Blinov DV, Bodikov VY, Mitrokhin SV, Volodin AA. Hydrogen storage and electrochemical properties of annealed low-Co AB5 type intermetallic compounds. Int J Hydrogen Energy 2021;46:13622–31. https://doi.org/10.1016/j.ijhydene.2020.12.071.